Clarification of Issues on the Closed-Form Green's Functions in Stratified Media

M. I. Aksun, *Senior Member, IEEE,* and Gülbin Dural, *Member, IEEE*

***Abstract*—The closed-form Green's functions (CFGF), derived for the vector and scalar potentials in planar multilayer media, have been revisited to clarify some issues and misunderstandings on the derivation of these Green's functions. In addition, the range of validity of these Green's functions is assessed with and without explicit evaluation of the surface wave contributions. As it is well-known, the derivation of the CFGF begins with the approximation of the spectral-domain Green's functions by complex exponentials, and continues with applying the Sommerfeld identity to cast these approximated spectral-domain Green's functions into the space domain in closed forms. Questions and misunderstandings of this derivation, which have mainly originated from the approximation process of the spectral-domain Green's functions in terms of complex exponentials, can be categorized and discussed under the topics of: 1) branch-point contributions; 2) surface wave pole contributions; and 3) the accuracy of the obtained CFGF. When these issues are clarified, the region of validity of the CFGF so obtained may be defined better. Therefore, in this paper, these issues will be addressed first, and then their origins and possible remedies will be provided with solid analysis and numerical demonstrations.**

***Index Terms*—Closed-form Green's function, discrete complex images method (DCIM), Green's function, multilayer media.**

I. Introduction

IT IS WIDELY accepted that the method-of-moments (MoM) based algorithms are the most suitable numerical algorithms for the rigorous analysis of layered printed structures of small to medium sizes (in terms of wavelength), when compared to other rigorous techniques like finite elements and finite-difference time domain methods [1]–[4]. For an application of MoM, one needs to write a governing equation in the form of an operator equation, which could be in the form of differential, integral or integro-differential operators [5]. Because the integral operators are more suitable for open geometries (not shielded), and because it is computationally more efficient for planar stratified media, the governing equation for the analysis and simulation of printed geometries in such media is formulated as a mixed-potential integral equation (MPIE) [6]. The application of the MoM for the solution of integral equations, either in spectral or spatial domain, requires the knowledge of the Green's functions in the corresponding domain. The Green's functions for multilayer media are traditionally represented by the Sommerfeld integrals in the spatial domain, and are obtained as closed-form expressions in the spectral domain. Although these representations of the Green's functions are well-known, they are not computationally efficient to use in conjunction with the MoM. This is mainly due to the oscillatory nature of the Sommerfeld integrals in the spatial domain, and due to slow-decaying nature of the spectral-domain Green's functions [7]. With this background in mind, following the introduction of the closed-form Green's functions (CFGF) in [8] and [9] for a printed geometry on a thick substrate, there have been several studies toward improving the approach and extending it to more general geometries [10]–[23]. All these studies on the efficient evaluation of the Green's functions in layered media have been motivated by the fact that printed geometries in multilayer environment have found increasingly more use in the designs of low-profile, light-weight and multifunction antennas, and microwave integrated circuits. Consequently, there has been a flurry of interest in developing computationally efficient computer-aided design tools for such geometries. In this context, the use of the CFGF in conjunction with the MoM has been a good candidate in developing an EM simulator to help analyze and design printed geometries [19].

Since printed geometries in multilayer media are, in general, formulated as MPIE, due to its less singular behavior as compared to other integral equation forms, the efficient calculations of Green's functions of vector and scalar potentials become necessary to be able to make the whole approach efficient and accurate. To achieve this goal—efficient calculation of the Green's functions—a new approach that transforms the integral representation of the spatial-domain Green's functions into closed-form expressions has been developed and improved recently [8]–[23]. This approach, which is named as the method of CFGF or discrete complex image method (DCIM), basically approximates the spectral-domain Green's functions in terms of complex exponentials and cast the integral representation into closed-form expressions via an integral identity, namely Sommerfeld identity [24]. Perhaps the crucial point of this approximation is that the approximating functions represent spherical waves with complex distances, referred to as complex images, and that dominant wave constituents of the fields of a dipole are spherical in nature. However, there are other wave constituents due to a dipole in a layered medium, like cylindrical and lateral waves, which may not be approximated in terms of complex images unless their contributions are explicitly accounted for. Hence, the CFGF may have some limitations in the form of a limited range of validity, where the range is defined as the distance of observation point from the source. Nevertheless, it provides a very accurate and efficient approximation for most practical problems that are within the range of validity of the

Manuscript received December 1, 2003; revised April 8, 2005.

M. I. Aksun is with the Department of Electrical and Electronics Engineering at Koc University, 34450 Sariyer- Istanbul, Turkey.

G. Dural is with the Department of Electrical and Electronics Engineering, Middle East Technical University, 06531 Ankara,Turkey (e-mail:gulbin@metu.edu.tr).

Digital Object Identifier 10.1109/TAP.2005.858571

approach, which is usually on the order of a few wavelengths. Beyond this range, the accuracy of the closed-form representations of the Green's functions becomes very poor unless all other wave types except the spherical ones have been extracted and explicitly treated. In the literature, this behavior was attributed to introducing nonphysical branch points into the approximated spectral-domain Green's functions in the process of approximation as performed in [8], [10] with the source embedded in an unbounded dielectric layer [12], [20], [22]. In addition, it is claimed that not extracting the quasidynamic terms in two-level approach causes some of the inaccuracies in the results [22]. However, the misinterpretation of the former claim was briefly discussed in [18] and the inaccuracy was attributed to the increased complexity due to the introduction of the extra branch cut. To eliminate any possible confusion on the inaccuracies and on the range of the use of CFGF, the following points are critically discussed with a view of their effects on the approximation of the Green's functions: 1) extraction of the quasistatic terms; 2) contributions of the branch points to Green's functions; and 3) contributions of the surface wave poles (SWP), and their extraction. Note that discussing these steps both from a mathematical and physical points of views provides definite answers to the questions on the steps of the DCIM and on its limitations, which can be considered as the main contribution of this paper. In addition, the study on the validity range of the DCIM with and without extracting the SWP is also the contribution of the paper. Note that this paper does not provide a new algorithm or method for the application of the DCIM as its contributions; rather it provides a thorough understanding of the technique, eliminates some lingering questions on the method, and provides qualitative and quantitative discussions on the range of application of the method, with and without a priory extraction of surface waves.

A brief overview of the development of the CFGF is given in Section II, in an itemized format that would help to clearly point out the difficulties, possible sources of errors and their remedies in the following sections. Then, the surface wave and branch point contributions are provided for a simple layered geometry in Section III, to demonstrate their region of influence as well as their approximations in term of complex exponentials. In Section IV, possible sources of errors, detailed discussions on the advantages, disadvantages, restrictions and range of validity, as well as some misunderstandings either caused by missing information in the previous papers, or caused by misinterpretations of certain numerical results are discussed. Finally, Section IV provides conclusion.

II. Brief Overview of DCIM

For the sake of illustration, consider a general planar-layered medium as shown in Fig. 1, where the source is above the interface between layer-i and layer-$(i-1)$ by a distance h. Moreover, to demonstrate the steps of getting CFGF and to point out the potential sources of problems, the scalar Green's function due to a horizontally oriented electric source, namely G_x^q, is chosen as the representative member of the Green's functions. As the spectral-domain representations of dyadic Green's functions have been derived and well-documented for layered media

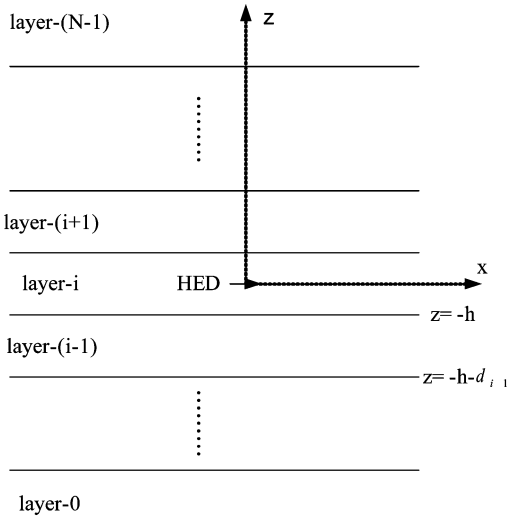

Fig. 1. Typical layered medium with an HED in layer-i.

[13], [16], [25], the one for the scalar potential is directly copied from [13] as

$$\tilde{G}_x^q = \frac{1}{2j\varepsilon_i k_{zi}}\left[e^{-jk_{zi}|z|} + \frac{k_{zi}^2 B_h^e + k_i^2 A_h^e}{k_\rho^2} e^{jk_{zi}z} + \frac{k_i^2 C_h^e - k_{zi}^2 D_h^e}{k_\rho^2} e^{-jk_{zi}z}\right] \quad (1)$$

where $k_{zi} = \sqrt{k_i^2 - k_\rho^2}$, and A_h^e, B_h^e, C_h^e and D_h^e are the functions of the generalized reflection coefficients $\tilde{R}_{\mathrm{TE,TM}}$ and the source location h. Note that, for the geometry depicted in Fig. 1 where layer-0 and layer-$(N-1)$ are semi-infinite dielectric media, there are two branch-point singularities in the spectral-domain expressions of the Green's functions, specifically at $k_\rho = k_{(0)}$ (k_0 is reserved for free-space while $k_{(0)}$ is for layer-0) and k_{N-1}, that is, at the wavenumbers of the outmost layers where one needs to consider the radiation condition for the choices of the branches of $k_{z(0)}$ and $k_{z(N-1)}$ [24]. In addition to the branch point singularities, there are some SWP between the minimum and maximum wavenumbers involved in the geometry, that is, in the range of $k_{\min}(= k_0\sqrt{\varepsilon_{r\,\min}}) < k_\rho < k_{\max}(= k_0\sqrt{\varepsilon_{r\,\max}})$. The number of SWP is dependent on the electrical thicknesses and dielectric constants of the layers involved.

The spatial-domain Green's functions are obtained either by using a two-dimensional transformation (inverse Fourier transform) or by employing a one-dimensional Hankel transformation of the corresponding spectral-domain Green's functions as

$$G_x^q = \frac{1}{4\pi}\int_{\mathrm{SIP}} dk_\rho k_\rho H_0^{(2)}(k_\rho\rho)\tilde{G}_x^q(k_\rho) \quad (2)$$

where SIP stands for Sommerfeld integration path and $H_0^{(2)}$ is the zeroth order Hankel function of second kind. Since both approaches involve in taking the integral of oscillatory and slow-convergent integrands, the method of obtaining CFGF in the spatial domain is nothing but approximating these integrals in closed-forms, efficiently and accurately. So, here are the steps

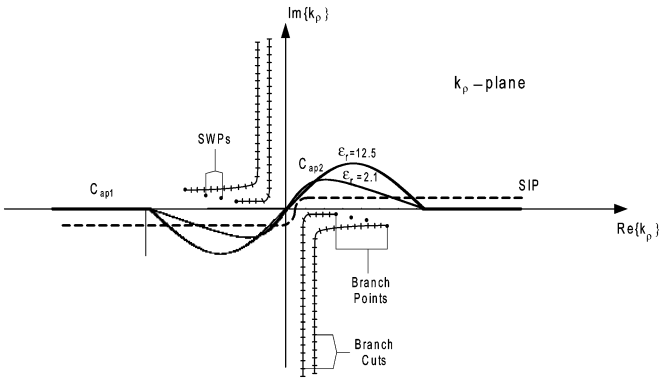

Fig. 2. Integration paths for the inversion of the spectral-domain Green's functions over k_ρ-plane, and some of the singularities.

of the method with some remarks, considering the spectral-domain Green's function given in (1) and following the two-level approach given in [15] the following.

1. **Sample the spectral-domain Green's function.** There are two approaches for this step: i) extract the spectral-domain representations of the quasistatic terms ($\tilde{G}_{\text{quasistatic}} = \lim_{k_0 \to 0} \tilde{G}$) and the surface-wave contributions ($\tilde{G}_{sw}$) analytically from the spectral-domain Green's function, and then sample the resulting function, $\tilde{G} - \tilde{G}_{\text{quasistatic}} - \tilde{G}_{sw}$; or ii) directly sample the terms in the square bracket for a constant z value in (1). The sampling for both approaches is performed over a path defined by the following mappings:

$$k_{zi} = -jk_i[T_{02} + t]$$
$$0 \le t \le T_{01} \quad \text{along} \quad C_{ap1} : 1^{\text{st}} \text{ level} \tag{3a}$$
$$k_{zi} = k_i\left[-jt + \left(1 - \frac{t}{T_{02}}\right)\right]$$
$$0 \le t \le T_{02} \quad \text{along} \quad C_{ap2} : 2^{\text{nd}} \text{ level} \tag{3b}$$

which is based on the two-level approach [15], but it could be extended to multilevel approach very easily [17]. The corresponding paths on k_ρ-plane and some of the features of the Green's functions, such as branch points, branch cuts and SWP, are shown in Fig. 2 for the sake of completeness and coherence of the discussions. It is well known that, in a layered medium, the branch points only exist at the wavenumbers of the outmost layers, i.e., at $k_\rho = k_{(0)}, k_{N-1}$ according to the geometry in Fig. 1, and the SWP exist between the minimum and maximum of the wavenumbers in the geometry.

Since the sampling path, denoted by C_{ap1} and C_{ap2} in Fig. 2, is a legitimately deformed path of SIP, the spectral-domain Green's function $\tilde{G}_x^q$ becomes a single-valued function of $k_{z(0)}$ and $k_{z(N-1)}$ over this path. Therefore, any function approximating the spectral-domain Green's function over this path can be considered as approximate and single-valued over the path. If the approximating function is not evaluated over the sampling path, neither approximation nor single-valuedness can be guaranteed. Note that the path C_{ap2} is drawn for two different dielectric media in Fig. 2, just to show the change in the path for different dielectric constants.

2. **Approximate the sampled spectral-domain Green's function by complex exponentials**, either using the Prony method (PM) or the generalized pencil-of-function method (GPOF), as

$$\tilde{G}_x^q \cong \tilde{G}_{xx}^{q0} + \tilde{G}_x^{qsw} + \underbrace{\frac{1}{j2\varepsilon_i k_{zi}}\left[\sum_{n=1}^{N_1} a_{1n} e^{-b_{1n}k_{zi}} + \sum_{n=1}^{N_2} a_{2n} e^{-b_{2n}k_{zi}}\right]}_{\cong \tilde{G}_x^q - \tilde{G}_x^{q0} - \tilde{G}_x^{qsw}} \tag{4a}$$

after having extracted the quasistatic terms $\tilde{G}_x^{q0}$ and the surface-wave contributions $\tilde{G}_x^{qsw}$ in spectral domain analytically, as noted in item 1. i), or as

$$\tilde{G}_x^q \cong \frac{1}{j2\varepsilon_i k_{zi}}\left[e^{-jk_{zi}|z|} + \sum_{n=1}^{N_1} a_{1n} e^{-b_{1n}k_{zi}} + \sum_{n=1}^{N_2} a_{2n} e^{-b_{2n}k_{zi}}\right] \tag{4b}$$

by directly sampling the spectral-domain Green's function as noted in item 1. ii). The coefficients a_{1n}, a_{2n}, and the exponents b_{1n}, b_{2n} in (4a) and (4b) are complex constants resulting from the application of the PM or GPOF method via the two-level sampling algorithm. Because both methods require uniform sampling over a real variable, and because the integration path for the inversion of the spectral-domain Green's functions, shown in Fig. 2, is over complex k_ρ-plane, it is necessary to introduce a mapping between the real variable "t" and the complex variable k_ρ, as defined in (3a) and (3b). Note that the multilevel sampling approach is employed to eliminate the restriction of uniform sampling. This is especially useful when the function to be approximated is smooth over a domain while it is fast changing over some other domain. It should also be noted that, since the GPOF method is more robust and less noise sensitive as compared to the PM [26], [27], the GPOF method is employed in this work.

3. **Get the closed-form spatial-domain Green's function from its approximated spectral-domain representation**, by using the Sommerfeld identity

$$\frac{e^{-jk_i r}}{r} = \int_{\text{SIP}} dk_\rho k_\rho H_0^{(2)}(k_\rho \rho) \times \frac{e^{-jk_{zi}|z|}}{j2k_{zi}} \quad \text{(Sommerfeld Identity)} \tag{5}$$

in the Hankel transformation defined in (2). Then, the following spatial-domain version of the Green's function is obtained:

$$G_x^q \cong G_x^{q0} + G_x^{qsw} + \frac{1}{4\pi\varepsilon_i}\left[\sum_{n=1}^{N_1} a_{1n}\frac{e^{-jk_i r_{1n}}}{r_{1n}} + \sum_{n=1}^{N_2} a_{2n}\frac{e^{-jk_i r_{2n}}}{r_{2n}}\right] \tag{6a}$$

$$G_x^q \cong \frac{1}{4\pi\varepsilon_i}\left[\frac{e^{-jk_i r}}{r} + \sum_{n=1}^{N_1} a_{1n}\frac{e^{-jk_i r_{1n}}}{r_{1n}} + \sum_{n=1}^{N_2} a_{2n}\frac{e^{-jk_i r_{2n}}}{r_{2n}}\right] \tag{6b}$$

where $r_{(1,2)n} = \sqrt{\rho^2 - b^2_{(1,2)n}}$ are complex in general, and hence this representation is also called DCIM. Note that (6a) and (6b) are the spatial-domain versions of (4a) and (4b), respectively, and that the quasistatic contributions G_x^{q0} for some simple geometry and the surface-wave contributions G_x^{qsw} can be found in closed-form in the spatial domain [8]–[10]. It should be stressed here that G_x^{q0} and G_x^{qsw} are obtained analytically from their spectral-domain representations, which are to be found analytically before the application of the DCIM.

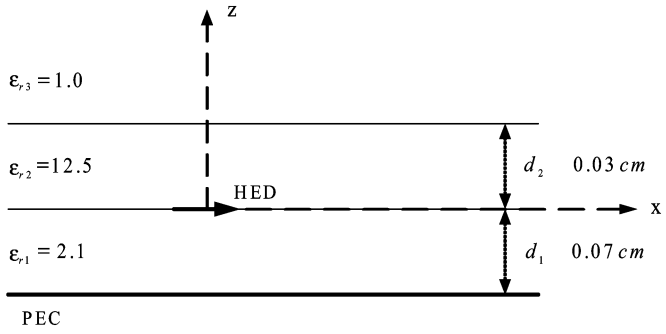

Fig. 3. Four-layer structure with an embedded HED.

III. Possible Problems and Their Sources

After the first introduction of the method that yields CFGF [8], [9], there have been plenty of discussions and improvements on the method, and applications of such representations of the Green's functions. The discussions have concentrated mainly on the approximation procedure, because the approximating CFGF are, in general, accurate enough for distances as far as $k_0\rho = 20{-}30\,(\rho/\lambda = 3{-}4)$, and beyond which they may deteriorate significantly. In this section, the attributed problems for the deterioration of the accuracy of the CFGF in the literature are discussed, and the sources of this inaccuracy together with the remedies, whenever possible, are demonstrated. There are basically three attributable sources of problems in the literature; one is about the part of the original method itself, and the others about the implementation of the two-level approach. These are, namely: i) introducing a wrong branch point in the process of approximation; ii) not extracting the quasistatic terms; and iii) not extracting the SWP in the implementation of two-level approach, respectively. These points are addressed in this section with a detailed discussion to clarify some misunderstandings.

A. Quasistatic Terms

This section is included to clarify the issue on whether the quasistatic terms need to be extracted explicitly in the implementation of the two-level approach, as suggested in [22], [23]. It should be remembered that the quasistatic terms are extracted from the spectral-domain Green's functions to make them convergent or fast convergent to zero for large k_ρ values, to eliminate the need of sampling the spectral-domain Green's functions over an extended range. Note that the quasistatic terms of a spectral-domain Green's function are obtained by finding the limiting terms as $k_\rho \to \infty$ (or $k_0 \to 0$) in the form of exponentials (real images). Therefore, in the application of the two-level approach, the approximation of the spectral-domain Green's functions on the path C_{ap1} via complex exponentials can be considered as the extraction of quasistatic terms in addition to some dynamic terms as well. In other words, once the approximation over the path C_{ap1} is subtracted from the spectral-domain Green's function, it can not only make the Green's function to smoothly converge to zero as $k_\rho \to \infty$ but it also makes it zero beyond a predefined value of k_ρ. In addition, derivation or finding the quasistatic terms analytically for a Green's function of an arbitrary geometry is quite difficult, if not impossible; therefore, the approximation performed over the path C_{ap1} in the two-level approach is designed specifically for this purpose, as well as for enabling two different frequencies of sampling.

To demonstrate the effectiveness of the two-level approach, a four-layer geometry is considered, as shown in Fig. 3: $f = 1$ GHz; layer-0: PEC; layer-1: $\varepsilon_{r1} = 2.1$, $d_1 = 0.07$ cm; layer-2: $\varepsilon_{r2} = 12.5$, $d_2 = 0.03$ cm; layer-3: free-space; HED is in Layer-2; $z = h = 0$. Note that this geometry is the same as the one studied in [12] at the frequency of 30 GHz, where it is claimed that the original approach of the closed-form Green's function suffers from introducing an artificial branch point when the source is in a bounded layer. This issue will be thoroughly discussed in Section III-B.

Extracting the exponentials that approximate a spectral-domain Green's function over large k_ρ makes the Green's function converge to zero, faster with the increased number of exponentials used, as demonstrated in Fig. 4(a) and (b). Therefore, approximation over the path C_{ap1} is much better than extracting the quasistatic terms, because it is robust, applicable for any number of layers, and automatic.

B. Discussion on Branch Point Singularities and Their Contributions

As it was mentioned above, for the geometry depicted in Fig. 1 where the source is in the bounded layer "i", the spectral-domain Green's functions have only two branch-point singularities at $k_\rho = k_{(0)}, k_{N-1}$, corresponding to the wavenumbers of uppermost and lowermost layers. Since mathematical and physical reasoning of this statement has been clearly given in [24], it is not discussed here any further. However, starting with [12], there have been a few discussions on the introduction of artificial branch points in the process of deriving the CFGF, and in turn, on the mathematical validity of the proposed approach in [8], [10] when used in a multilayer environment with the source buried into a bounded layer [20], [22].

The issue of incorrect complex-plane topology (due to artificial introduction of a branch point) was raised with an observation that the approximated scalar Green's function, as obtained using the approach in [8], [10], is violently off as compared to the exact Green's function for the geometry given in Fig. 3 where HED is positioned in Layer-2 [12], even for small distances from the source. According to the plot, Fig. 10 in [12], the deviation between the approximation and the quadrature begins around $\rho \geq 0.02\lambda$. However, with the applications of the two-level approach without the modification proposed in [12], for HED in Layer-2 and in Layer-1, the deviation stars beyond

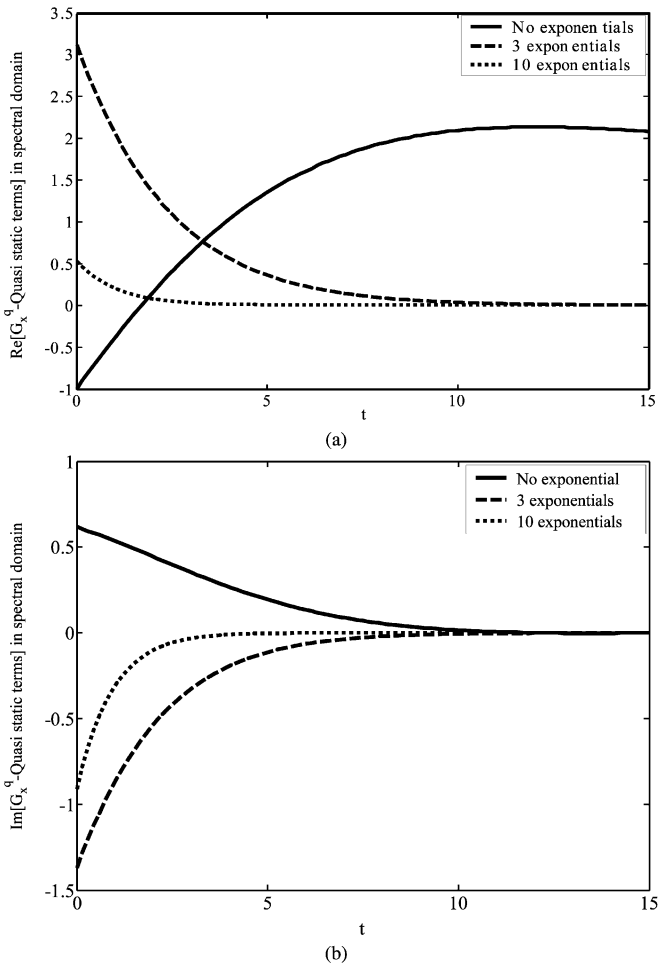

Fig. 4. (a) Real and (b) imaginary parts of the effect of subtracting the exponentials of 1st level approximation over C_{ap1} (quasistatic terms) from the spectral-domain Green's function $\bar{G}_x^q$ sampled over C_{ap2}.

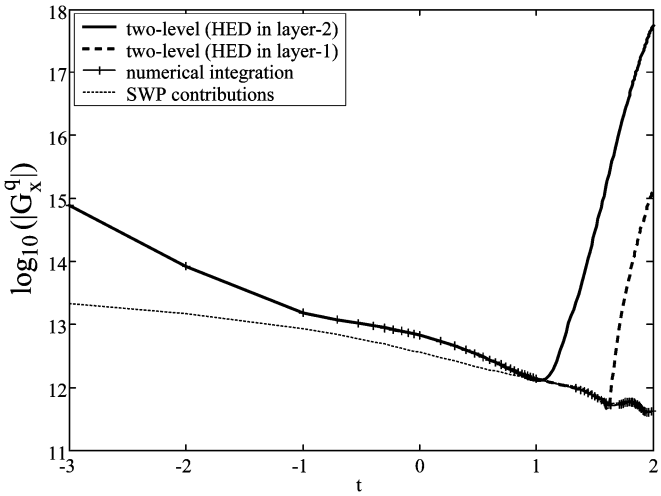

Fig. 5. Magnitude of the scalar Green's function (approximate and exact), and the surface wave contribution for the geometry in Fig. 3.

$\rho \geq 1.59\lambda$ and $\rho \geq 6\lambda$, respectively, as demonstrated in Fig. 5, which are significant improvements over the data provided in [12]. Note that the source HED at the interface can be considered either in layer-1 or in layer-2 as the interface can be modeled as the part of layer-1 or layer-2, respectively. The difference in accuracy observed may be attributed to the use of the

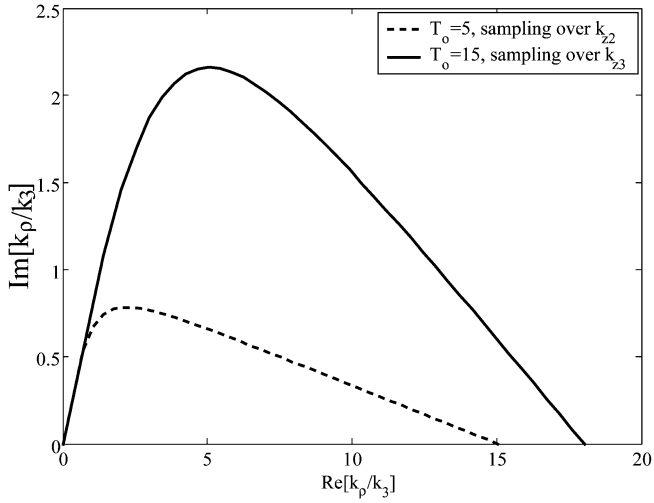

Fig. 6. Deformed integration paths over k_ρ/k_0- plane corresponding to the sampling over $k_{z2} = k_2[-jt + (1 - t/T_0)]$ for $T_0 = 5$, and $k_{z3} = k_3[-jt + (1 - t/T_0)]$ for $T_0 = 15$. Note that $k_3 = k_0$ for the geometry given in Fig. 3.

Prony method in [12], and not using enough samples for small k_ρ values when the original approach was used.

For the original Prony method, it has already been demonstrated that it is very noise sensitive [26], [27], and alternative methods, like the least-square Prony and the GPOF methods, have been proposed. So, this issue is not detailed here any further. However, for the sampling issue, which seems to be the key factor for the early deterioration of the approximated Green's functions in [12], it would be instructive to give a few sentences more. Note that the Green's functions compared in Fig. 10 in [12] were obtained by implementing the method with the sampling performed over the path of k_ρ using k_{z2} and k_{z3} mappings, as given in (3a) and (3b) for k_{zi} mapping. Remember that sampling over the path of k_ρ using k_{z3} mapping, even though the source is in layer-2, has been made possible with the modification of the original approach by multiplying the numerator and denominator of the spectral-domain Green's function by k_{z3}, i.e., k_z of the outmost medium [12]. The actual integration paths over k_ρ-plane for the choices of the following mappings are shown in Fig. 6:

$$k_{z3} = k_3\left[-jt + \left(\frac{1-t}{T_0}\right)\right] \quad \text{for} \quad T_0 = 15 \tag{7a}$$

$$k_{z2} = \underbrace{k_3\sqrt{12.5}}_{k_2}\left[-jt + \left(\frac{1-t}{T_0}\right)\right] \quad \text{for} \quad T_0 = 5 \tag{7b}$$

where the same number of samples, 41 in this case, over the corresponding ranges is used.

Note that, since k_2 is $\sqrt{12.5}$ times larger than $k_3 (= k_0)$, the sampling range for the mapping function of k_{z2} is reduced to 5 from 15 to bring the maximum of $\mathrm{Re}(k_\rho)$ to the same neighborhood. Although this adjustment of the sampling range T_0 provides similar ranges on k_ρ-plane for both mappings, it cannot provide a similar set of sampling points, especially for small k_ρ values, as evidenced from Fig. 6. To put this into numbers, the first samples for both cases are at zero, and the second ones are at $k_\rho/k_3 = (0.6876 + j0.5318)$ and $k_\rho/k_3 = (1.4082 + j1.0819)$

for the mapping functions of k_{z3} and k_{z2}, respectively. Therefore, with the sampling using k_{z2}, the fine features of the function to be approximated, for small k_ρ values, are not properly accounted for, which results in a poor approximation in the spatial domain for moderate to large values of ρ. This example demonstrates that the choice of k_z for the definition of the path in k_ρ-plane is very important to have enough samples of the Green's function over the chosen path to get a good exponential approximation. Therefore, one may use the modification proposed in [12] to change the path. The modification is nothing but multiplying and dividing the spectral-domain Green's function by k_z of the layer with lowest dielectric material (k_z of the free-space that coincides with the branch point in most practical problems) and choosing this k_z to define the path and the exponential expansion.

Let us look at this issue from the mathematical point of view. The spectral-domain Green's function, $\tilde{G}_x^q$ in this work, has branch points at $\pm k_3$ ($= k_0$, free-space wave number) and associated branch-cuts, not counting the branch point of Hankel function at $k_\rho = 0$. Once these branch-cuts are specified, the integration path of the Sommerfeld integral can be deformed to avoid these branch-cuts, and therefore, the integrand becomes a single valued function of k_{z3} $\left(= \sqrt{k_3^2 - k_\rho^2}\right)$ over the deformed integration path. The path used for the exponential approximation, defined by (7a) or (7b), is one of such paths, and hence the functions to be approximated by complex exponentials along any one of these paths, as well as the approximating functions, are single valued. Subsequently, the Sommerfeld identity can be used, with no problem, for these approximating functions.

Another point is that the branch-point contribution at the interfaces behaves like $1/\rho^2$, while the surface wave contribution behaves as $1/\sqrt{\rho}$. In other words, the branch point contribution decays much faster than the contributions of the SWP. With a little examination of Fig. 5, it is seen that the deviations for both cases can occur where the surface wave contribution stars dominating the Green's function, which should be way out of the influence range of the branch-point contribution.

C. Effects of the SWP Contributions on the DCIM

As the conclusion of the previous section, the surface wave pole contributions seem to be responsible for the violent deterioration of the approximation for moderate distances from the source. To verify this conclusion, a three-layer geometry, as shown in Fig. 7, is studied at the frequency of 1 GHz, for which there is only one TM surface wave pole at $k_{\rho p} = 0.21\ \mathrm{rad/cm}$.

The two-level approach is used to get the closed-form Green's function for the scalar potential, for the case that HED is at interface between layer-1 and layer-2. Since the scalar potential is continuous across the interface, HED could be considered at the interface in layer-1 or in layer-2, resulting in two different spectral-domain representations of the same Green's function. Considering the differences in sampling paths for these cases, as demonstrated in Fig. 6 for another geometry, the quality of approximation of these spectral-domain Green's functions may be significantly different. It is observed that the approximations for both cases fail to approximate the true nature of the Green's function for large distances from the source, as given in Fig. 8.

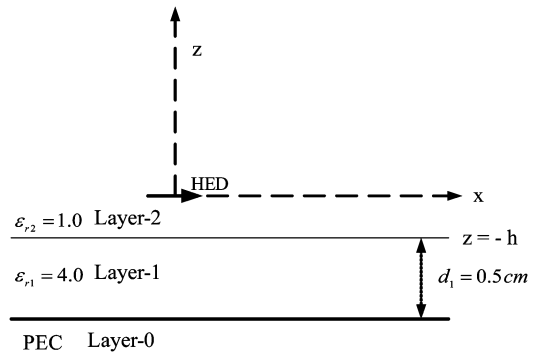

Fig. 7. Three-layer geometry.

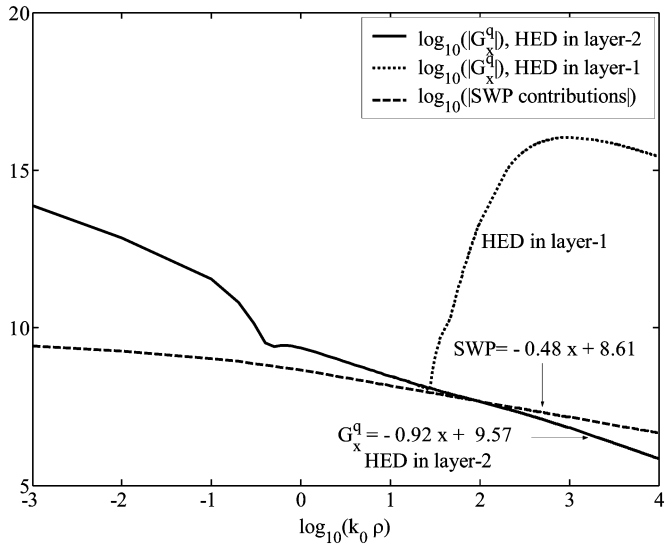

Fig. 8. Magnitude of the scalar Green's function and the SWP contribution for the geometry given in Fig. 7. $f = 1.0$ GHz; HED is at interface in Layer-1 and in Layer-2, $h = 0.5$ and 0.0 cm, respectively.

It is obvious that the deviation of the approximation is much more pronounced when HED is in layer-1 than that when it is in layer-2. However, it is clear that neither approximation predicts the dominant behavior of the SWP, as shown in Fig. 8 where the SWP contribution and the approximation (HED in layer-2) are line-fitted. While the fitted line for the surface wave contribution has approached to its theoretical limit ($1/\sqrt{\rho}$ of a slope of -0.5 on a log-log scale), the one for the approximation has approached to the limit of the spherical wave ($1/\rho$ of a slope of -1.0 on a log-log scale), as given by the equations in Fig. 8. Since the approximating functions, complex images, are spherical waves coming from complex distances, the behavior of the approximating functions is expected, except for the drastic increase of the magnitude of the Green's function in almost far-field zone. This anomalous behavior will be further investigated in this section right after the discussion of SWP contribution and its spherical wave approximations. Remembering that the failure of DCIM in rather near-field region has been attributed to poor sampling in the case of HED in layer-1 in Section III-B, it is of paramount importance to distinguish the problems in the application of the DCIM from the inherent problems of the approximation method. Since the functional behavior of the approximating and approximated functions are different for large ρ values at the interface, $1/\rho$ and $1/\sqrt{\rho}$, respectively, the

failure of the DCIM at large distances could be due to this inherent problem of the method. Therefore, the approximation of SWP contributions in terms of complex images needs to be investigated by trying to approximate the SWP contributions via spherical waves.

Note that the first step to find the SWP contribution for the Green's function is to find the SWP(s), then, the contribution is obtained by taking the following integral analytically:

$$G_{qsw}^{x} = \frac{1}{4\pi\varepsilon} \times \sum_{i=1}^{N_{\mathrm{TE}}+N_{\mathrm{TM}}} \int_{\mathrm{SIP}} dk_\rho k_\rho H_0^{(2)}(k_\rho\rho) \left[\frac{2k_{\rho p(i)}\mathrm{Res}^{(i)}}{k_\rho^2 - k_{\rho p(i)}^2}\right] \quad (8)$$

where $k_{\rho p(i)}$ and $\mathrm{Res}^{(i)}$ are the ith SWP and corresponding residue. Since the term in the square bracket can be recognized as the spectral-domain representation of the SWPs, by comparing it to (2), it is a straightforward application of the two-level approach to approximate this term by complex exponentials. Once this is approximated by complex exponentials, using the Sommerfeld identity would provide a set of spherical waves approximating the SWP contributions, which are actually cylindrical waves. To perform the GPOF for the term in the square bracket, it should be noted that the terms in the numerator are constants, and that one needs $1/j2k_z$ term for the application of the Sommerfeld identity. Therefore, the term in the square bracket in (8) is multiplied and divided by $j2k_z$, resulting in

$$G_{qsw}^{x} = \frac{1}{4\pi\varepsilon} \sum_{i=1}^{N_{\mathrm{TE}}+N_{\mathrm{TM}}} 2k_{\rho p(i)}\mathrm{Res}^{(i)} \times \int_{\mathrm{SIP}} dk_\rho k_\rho H_0^{(2)}(k_\rho\rho) \frac{1}{j2k_z} \frac{j2k_z}{k_\rho^2 - k_{\rho p(i)}^2}. \quad (9)$$

Now the function $(j2k_z/k_\rho^2 - k_{\rho p(i)}^2)$ is approximated in terms of exponentials of k_z as follows:

$$\frac{j2k_z}{k_\rho^2 - k_{\rho p(i)}^2} = \sum_{n=1}^{N\exp} b_{\mathrm{in}} e^{-\beta_{\mathrm{in}} k_z} \quad (10)$$

where b_{in} and β_{in} are the coefficients and exponents for the ith SWP, respectively. Hence, the SWP contribution can be obtained in terms of spherical waves as

$$G_{qsw}^{x} = \frac{1}{4\pi\varepsilon} \sum_{i=1}^{N_{\mathrm{TE}}+N_{\mathrm{TM}}} 2k_{\rho p(i)}\,\mathrm{Res}^{(i)} \sum_{n=1}^{N\exp} b_{\mathrm{in}} \frac{e^{-jr_{\mathrm{in}}}}{r_{\mathrm{in}}} \quad (11)$$

where $r_{\mathrm{in}} = \sqrt{\rho^2 - \beta_{\mathrm{in}}^2}$ and $k^2 = k_\rho^2 + k_z^2$. The spherical wave approximation of the SWP contribution and the SWP contribution itself are given in Figs. 9 and 10, for HED in layer 2 and in layer-1, respectively. Note that k_{z2} and k_{z1} are used in (10) for the cases of HED in layer-2 and HED in layer-1, respectively. The DCIM approximation of the scalar Green's function G_x^q is also given for both cases to see and to compare the deviations in the approximation of the SWP contribution and the approximation of the Green's function. It is obvious from Figs. 9 and 10 that the deviations of the approximations of the Green's function start at the distances where the spherical wave approximations of the SWP contribution deviate from the exact SWP contribution.

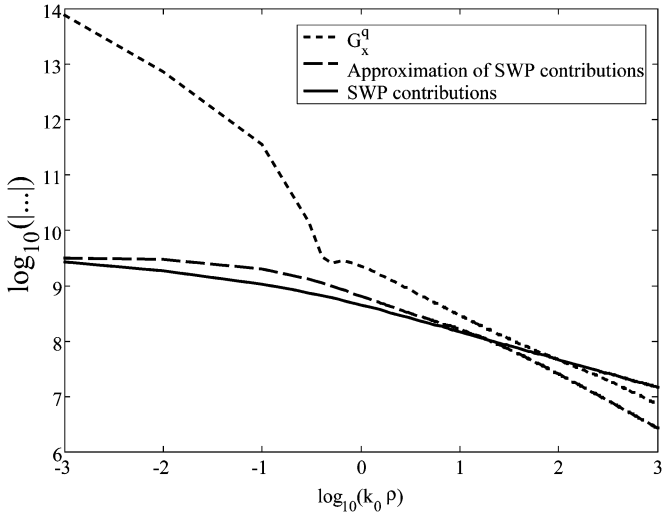

Fig. 9. Magnitudes of the SWP contribution and its spherical wave expansion, for the geometry shown in Fig. 7. Source and observation are in medium 2, $z = h = 0$, $f = 1.0$ GHz.

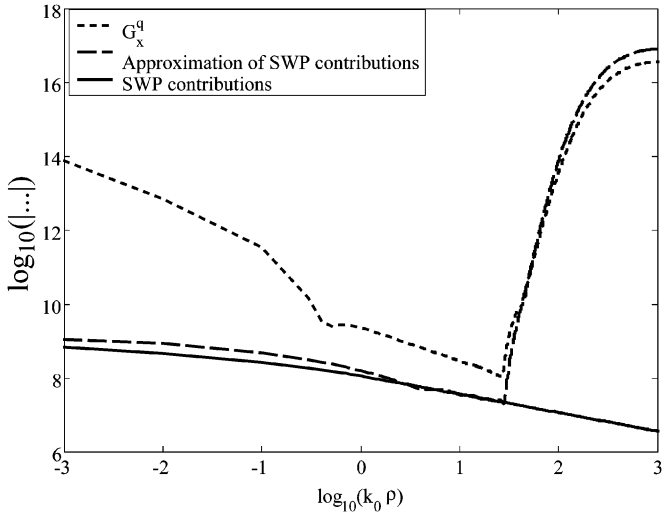

Fig. 10. Magnitudes of the SWP contribution and its spherical wave expansion, for the geometry shown in Fig. 7. Source and observation are in medium 1, $z = 0, h = 0.5$, $f = 1.0$ GHz.

There is one more question left to be answered: why are the approximations of SWP contribution and the Green's function for the case of HED in layer-2 behave much milder as compared to those for HED in layer-1? Is it because the Sommerfeld identity is not applicable for the exponentials that GPOF provides, at least for some of them, and in turn the resulting exponentials cannot represent spherical waves that decay for large distances from the source?

To answer these questions, one needs to remember that the sampled values of the spectral-domain Green's functions for both cases are very different, especially near origin, which is due to sampling over different paths, as shown in Fig. 6, and a slight

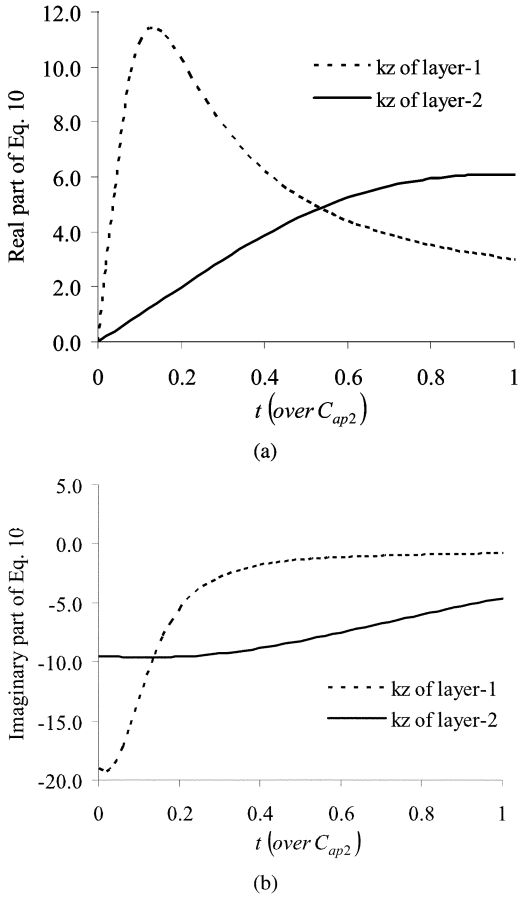

Fig. 11. (a) Real and (b) imaginary parts of (10), the spectral-domain representation of the SWP Contribution, for the geometry in Fig. 7 $k_{\rho p} = 0.21\ \mathrm{rad/cm}$, $f = 1.0\ \mathrm{GHz}$.

difference in the functions to be approximated, just different k_z's. It may be easier to imagine and to accept the fact that the spectral-domain Green's functions can be significantly different for different choices of the sampling path, as they are quite complex functions. However, the spectral-domain representation of the surface-wave contribution, (10), is rather simple, but its spatial-domain approximations in terms of spherical waves still show significant difference when the path of sampling is changed, Figs. 9 and 10. So, to understand the source of rather significant difference in the spatial-domain behavior of the SWP contributions due to such simple changes, the spectral-domain values, (10), along the paths defined by k_{z1} and k_{z2} are given in Fig. 11(a) and (b). Note that, for Fig. 11(a) and (b), (10) is sampled only on the path C_{ap2} with the choice of $T_{02} = 4$ and the number of samples of 201, as these parameters define the path of sampling in addition to the choice of k_z. It is obvious from these curves that the sampled data for the path associated with k_{z1} (k_z of layer-1) are more difficult to approximate, especially to capture the fast varying part near the origin, than those for the path associated with k_{z2}.

To answer the question whether the Sommerfeld identity is applicable for the exponentials obtained from the approximation when HED is in layer-1, these exponentials, as well as the exponentials for the case of HED being in layer-2, are given in Table I. Note that these exponentials are only for the second level of the two-level algorithms, since the approximations in the first level, over C_{ap1}, always provide smoothly decaying exponentials. It is obvious from Table I that the first 2–3 exponentials for the case of HED in layer-1 have very large coefficients and exponents, as compared to the rest of the exponentials for both cases. Although it was clear from the derivation of the Sommerfeld identity that the only requirement to use this identity is to have a k_z with negative imaginary part [24], [28], to eliminate any lingering question, the Sommerfeld identity has been verified numerically for such exponentials. As a result, it was observed that these contributions in the spatial domain behave exactly the same way as predicted by the Sommerfeld identity, that is, as spherical waves. The only difference for these images with large coefficients and exponents is that they have their maximum somewhere in the middle range (around $k_0\rho \geq 10$) rather than the origin ($k_0\rho = 0$). If the algorithm is to employ more exponential terms to improve accuracy along the path C_{ap2}, as it is the case for HED in layer-1 due to fast changes near the origin of k_ρ-plane, it may improve the spatial-domain Green's function for moderate values of ρ at the cost of violent deterioration beyond. As it was mentioned already, this deterioration is mainly due to the incompatibility of the natures of approximating and approximated functions, spherical and cylindrical waves, respectively.

Up to this point, it has been discussed that approximations fail to approximate the true nature of the Green's functions for large distances from the source mainly because of two reasons: 1) poor sampling and the sampling frequency and 2) trying to approximate SWP contributions by using spherical waves. The former can be improved by changing the parameters of the approximation algorithm, but the latter is inherent to the approach unless the SWP contributions are totally extracted from the functions to be approximated. To eliminate this rather inherent problem of poor approximation of SWP contributions via spherical waves, it may be suggested to subtract the SWP from the spectral-domain Green's functions before the approximation, and to add their contribution analytically after the approximation. This approach, when used in conjunction with the two-level or multilevel DCIM, eliminates all the problems involved in casting the Green's functions in closed forms for any distance from the source, as demonstrated in Fig. 12. However, although finding the SWPs and the associated residues for the frequencies of interest are quite easy and robust [21], keeping all complex images (about 30 exponentials for each Green's function involved in the MPIE formulation) in the implementation of the MoM for large problems may become computationally very expensive. As it is observed from Fig. 12 and stated in [15], the Green's functions behave exactly like SWP contributions beyond a certain distance, so using the CFGF up to a certain distance, without extracting the SWP contributions, and using only the SWP contributions beyond a certain distance would be sufficient. Since the common goal of getting the CFGF is to use them in the application of MoM, this approach eliminates any special treatment of the Hankel function in the SWP contribution in near-field regions [29], and eliminates the total number of complex images in the calculation of the MoM matrix entries beyond the switching distance. This switching distance can easily be defined adaptively during the process of calculating the MoM matrix entries.

TABLE I
COEFFICIENTS AND EXPONENTS OF COMPLEX EXPONENTIALS FOR THE APPROXIMATION OF $\bar{G}_x^q$ OVER C_{ap2} ONLY, FOR THE GEOMETRY IN FIG. 7

HED in Layer-1			HED in Layer-2		
	Coefficient (a_{2n})	Exponent (b_{2n})		Coefficients (a_{2n})	Exponent(b_{2n})
1	299034409+j 559243726	61.96+j 184.57	1	0.0+j 0.0	-496+j 1588
			2	0.009+j 0.014	59.85+j 60.3
2	-479.4-j 1867.2	28.3+j 124.6	3	0.0009+j 0.009	39.1+j 49.2
3	-3.23-j 3.53	12.59+j 88.2	4	-0.0014+j 0.0055	25.5+j 39.7
4	0.0898+j 0.235	5.12+j 62.9	5	-0.0019+j 0.0034	15.96+j 31.4
5	0.026+j 0.05	1.56+j 45.0	6	-0.0018+j 0.002	9.28+j 24.04
6	-0.025+j 0.007	0.06+j 32.3	7	-0.0015+j 0.0012	4.67+j 17.73
7	0.023-j 0.0077	0.067+j 23.1	8	0.0+j 0.0	-4.73+j 7.08
8	-0.032+j 0.001	0.59+j 15.25	9	0.0+j 0.0	5.13+j 7.45
9	0.0+j 0.0	-1.40-j 1.96	10	-0.0002+j 0.0	-2.31+j 9.76
10	0.011-j 0.0007	-1.12+j 8.89	11	-0.0014+j 0.0007	1.47+j 12.2
11	0.0-j 0.0001	-2.99+j 4.48	12	1.0+j 0.0	0.0+j 0.0
12	0.0026-j 0.005	-1.92+j 6.21			
13	0.0039+j 0.0079	1.75+j 6.53			
14	0.0+j 0.0001	3.47+j 4.64			
15	1.0+j 0.0	0.0+j 0.0			

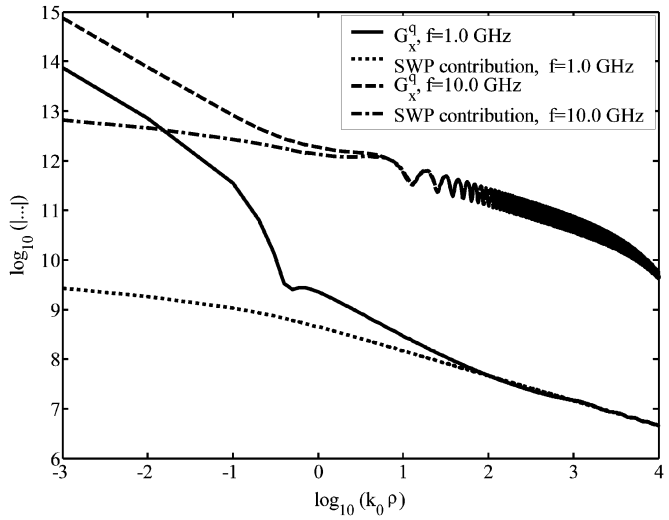

Fig. 12. Magnitudes of the scalar Green's function and the SWP contribution for the geometry given in Fig. 7. Green's functions are obtained by first extracting the SWPs in the spectral-domain and adding their contributions in the spatial-domain analytically. $z = h = 0$ (HED is at interface).

IV. CONCLUSION

In this paper, the CFGF, derived for the vector and scalar potentials using DCIM, for planarly layered media have been revisited to clarify some issues and misunderstandings on the use of the DCIM. In the literature, there have been mainly three attributable problems in the implementations of the original method and its modified version, the multilevel DCIM: 1) not extracting quasistatic terms in the two-level DCIM; 2) introducing a wrong branch point in the process of approximation; and 3) not extracting the SWP in the implementation of two-level approach. These issues have been addressed from both theoretical and practical points of views, and the following conclusions have been drawn: i) no need to extract quasistatic terms in the use of two-level or multilevel DCIM, because the first level actually extracts the quasistatic terms and more; ii) no introduction of wrong branch points, as the path of integration is the legitimately deformed path from SIP and over which the integrands are single-valued functions; iii) extraction of SWPs is not necessary if the Green's functions are to be used in the application of MoM, nevertheless the contributions of SWPs need to be calculated in order to be used in the places of Green's functions wherever the SWP contributions dominate. Of course, the last conclusion is for the efficient use of the CFGF in the MoM procedure.

REFERENCES

[1] M. J. Tsai, F. D. Flavis, O. Fordharn, and N. G. Alexopoulos, "Modeling planar arbitrarily shaped microstrip elements in multilayered media," *IEEE Trans. Microw. Theory Tech.*, vol. 45, no. 3, pp. 330–337, Mar. 1997.

[2] M. R. Abdul-Gaffoor, H. K. Smith, A. A. Kishk, and A. W. Glisson, "Simple and efficient full-wave modeling of electromagnetic coupling in realistic RF multilayer PCB layouts," *IEEE Trans. Microw. Theory Tech.*, vol. 50, no. 6, pp. 1445–1457, Jun. 2002.

[3] J. Yeo and R. Mittra, "An algorithm for interpolating the frequency variations of method-of-moments matrices arising in the analysis of planar microstrip structures," *IEEE Trans. Microw. Theory Tech.*, vol. 51, no. 3, pp. 1018–1025, Mar. 2003.

[4] E. A. Soliman, M. H. Bakr, and N. K. Nikolova, "Neural networks-method of moments (NN-MoM) for the efficient filling of the coupling matrix," *IEEE Trans. Antennas Propag.*, vol. 52, no. 6, pp. 1521–1529, Jun. 2004.

[5] R. F. Harrington, *Field Computations by Moment Methods*. New York: Macmillan, 1968.

[6] J. R. Mosig, "Arbitrarily shaped microstrip structures and their analysis with a mixed potential integral equation," *IEEE Trans. Microw. Theory Tech.*, vol. MTT-36, no. 2, pp. 314–323, Feb. 1988.

[7] M. I. Aksun and R. Mittra, "Choices of expansion and testing functions for the method of moments in electromagnetic problems," *IEEE Trans. Microw. Theory Tech.*, vol. MTT-41, no. 3, pp. 503–509, Mar. 1993.
[8] D. C. Fang, J. J. Yang, and G. Y. Delisle, "Discrete image theory for horizontal electric dipoles in a multilayered medium," *Proc. Inst. Elect. Eng.*, pt. H, vol. 135, pp. 297–303, Oct. 1988.
[9] Y. L. Chow, J. J. Yang, D. G. Fang, and G. E. Howard, "A closed-form spatial Green's function for the thick microstrip substrate," *IEEE Trans. Microw. Theory Tech.*, vol. 39, no. 3, pp. 588–592, Mar. 1991.
[10] M. I. Aksun and R. Mittra, "Derivation of closed-form Green's functions for a general microstrip geometry," *IEEE Trans. Microw. Theory Tech.*, vol. MTT-40, no. 11, pp. 2055–2062, Nov. 1992.
[11] ——, "Estimation of spurious radiation from microstrip etches using closed-form Green's functions," *IEEE Trans. Microw. Theory Tech.*, vol. MTT-40, no. 11, pp. 2063–2069, Nov. 1992.
[12] R. A. Kipp and C. H. Chan, "Complex image method for sources in bounded regions of multilayer structures," *IEEE Trans. Microw. Theory Tech.*, vol. 42, no. 5, pp. 860–865, May 1994.
[13] G. Dural and M. I. Aksun, "Closed-Form Green's functions for general sources and stratified media," *IEEE Trans. Microw. Theory Tech*, vol. 43, no. 7, pp. 1545–1552, Jul. 1995.
[14] K. A. Michalski and J. R. Mosig, "Discrete complex image mixed-potential integral equation analysis of microstrip patch antennas with vertical probe feeds," *Electromagn.*, vol. 15, pp. 377–392, 1995.
[15] M. I. Aksun, "A robust approach for the derivation of closed-form Green's functions," *IEEE Trans. Microw.Theory Tech.*, vol. 44, no. 5, pp. 651–658, May 1996.
[16] K. A. Michalski and J. R. Mosig, "Multilayered media Green's functions in integral equation formulations," *IEEE Trans. Antennas Propag.*, vol. 45, no. 3, pp. 508–519, Mar. 1997.
[17] N. Kinayman and M. I. Aksun, "Efficient use of closed-form Green's functions for the analysis of planar geometries with vertical connections," *IEEE Trans. Microw. Theory Tech.*, vol. 45, no. 5, pp. 593–603, May 1997.
[18] N. Hojjat, S. Safavi-Naeini, and Y. L. Chow, "Numerical computation of complex image Green's functions for multilayer dielectric media: Near-Field zone and the interface region," *Proc. Inst. Elect. Eng.-Microw. Antennas Propag.*, vol. 145, pp. 449–454, Dec. 1998.
[19] N. Kinayman and M. I. Aksun, *EMPLAN: Electromagnetic Analysis of Printed Structures in Planarly Layered Media*. Norwood, MA: Artech House, 2000.
[20] J. Bernal, F. Medina, R. R. Boix, and M. Horno, "Fast full-wave analysis of multistrip transmission lines on mpie and complex image theory," *IEEE Trans. Microw. Theory Tech.*, vol. 48, no. 3, pp. 445–452, Mar. 2000.
[21] F. Ling and J. M. Jin, "Discrete complex image method for Green's functions of general multilayer media," *IEEE Trans. Microw. Guided Wave Lett.*, vol. 10, pp. 400–402, Oct. 2000.
[22] J. Bernal, F. Medina, and R. R. Boix, "Full-Wave analysis of nonplanar transmission lines on layered medium by means of MPIE and complex image theory," *IEEE Trans. Microw. Theory Tech.*, vol. 49, no. 1, pp. 177–185, Jan. 2001.
[23] N. V. Shuley, R. R. Boix, F. Medina, and M. Horno, "On the fast approximation of Green's functions in MPIE formulations for planar layered media," *IEEE Trans. Microw. Theory Tech.*, vol. 50, no. 9, pp. 2185–2192, Sep. 2002.
[24] W. C. Chew, *Waves and Fields in Inhomogeneous Media*, ser. Electromagnetic Waves. New York: IEEE Press, 1995.
[25] N. K. Das and D. M. Pozar, "A generalized spectral-domain Green's function for multilayer dielectric substrates with application to multilayer transmission lines," *IEEE Trans. Microw. Theory Tech.*, vol. 35, no. 3, pp. 326–335, Mar. 1987.
[26] Y. Hua and T. K. Sarkar, "Generalized pencil-of-function method for extracting poles of an EM system from its transient response," *IEEE Trans. Antennas Propag.*, vol. AP-37, no. 2, pp. 229–234, Feb. 1989.
[27] A. J. Mackay and A. McCowen, "An improved pencil-of-function method and comparisons with traditional methods of pole extraction," *IEEE Trans. Antennas Propag.*, vol. AP-35, no. 4, pp. 435–441, Apr. 1987.
[28] D. G. Dudley, *Mathematical Foundations for Electromagnetic Theory*, ser. Electromagnetic Waves. New York: IEEE Press, 1994.
[29] F. Demuynck, G. A. E. Vandenbosch, and A. R. Van den Capelle, "The expansion of wave concept—Part I: Efficient calculation of spatial Green's functions in stratified dielectric medium," *IEEE Trans. Antennas Propag.*, vol. 46, no. 3, pp. 397–406, Mar. 1998.

M. I. Aksun (M'92–SM'99) received the B.S. and M.S. degrees in electrical and electronics engineering at the Middle East Technical University, Ankara, Turkey, in 1981 and 1983, respectively, and the Ph.D. degree in Electrical and computer engineering at the University of Illinois at Urbana-Champaign, in 1990.

From 1990 to 1992, he was a Postdoctoral Fellow in the Electromagnetic Communication Laboratory at the University of Illinois at Urbana-Champaign. From 1992 to 2001, he was on the faculty of the Department of Electrical and Electronics Engineering at Bilkent University, Ankara, Turkey, where he was a Professor since 1999. In 2001, he has joined the Department of Electrical and Electronics Engineering at Koc University, Istanbul, Turkey, as a professor, and starting in May 2004, he has been serving as the Dean of Engineering College. His research interests include numerical methods for electromagnetics and optics, printed circuits and antennas, and indoor and outdoor propagation models.

Gülbin Dural (S'85–M'88) received the B.S. and M. S. degrees in electrical and electronics engineering from the Middle East Technical University, Ankara, Turkey, in 1981 and 1983, respectively, and the Ph.D. degree from The Ohio State University, Columbus, in 1988.

From 1981 to 1983, she was with the Department of Electrical Engineering, Middle East Technical University, as a Graduate Assistant, and from 1984 to 1988, she was with the ElectroScience Laboratory, Ohio State University, as a Graduate Research Associate. Since 1989, she has been on the faculty of Department of Electrical and Electronics Engineering at the Middle East Technical University, where she is currently a Professor. Between 2000 and 2004, she also served as the Assistant Director of Scientific and Technical Research Council of Turkey- Information Technologies and Electronics Research Institute (TÜBITAK-BILTEN). Her research interests include the numerical methods for electromagnetics, microstrip antennas, microwave and millimeter-wave integrated circuits, and SAR and ISAR imaging techniques.